

Efficient Computation of Whole-Body Control Utilizing Simplified Whole-Body Dynamics via Centroidal Dynamics

Junewhee Ahn¹, Jaesug Jung², Yisoo Lee³, Hokyun Lee¹, Sami Haddadin⁴ and Jaeheung Park^{1,5}

Abstract—In this study, we present a novel method for enhancing the computational efficiency of whole-body control for humanoid robots, a challenge accentuated by their high degrees of freedom. The reduced-dimension rigid body dynamics of a floating base robot is constructed by segmenting its kinematic chain into constrained and unconstrained chains, simplifying the dynamics of the unconstrained chain through the centroidal dynamics. The proposed dynamics model is possible to be applied to whole-body control methods, allowing the problem to be divided into two parts for more efficient computation. The efficiency of the framework is demonstrated by comparative experiments in simulations. The calculation results demonstrate a significant reduction in processing time, highlighting an improvement over the times reported in current methodologies. Additionally, the results also shows the computational efficiency increases as the degrees of freedom of robot model increases.

I. INTRODUCTION

The field of humanoid robotics has witnessed significant advances in recent years, driven by the demand for robots that can operate in environments designed for humans and perform tasks ranging from simple repetitive actions to complex, dynamic interactions. One of the essential components in realizing it is the development of Whole-Body Control (WBC) frameworks, as initially explored in foundational research [1], [2]. WBC facilitates the execution of multi-task control at the torque level within the operational space, carefully accounting for contact dynamics and ensuring consistency with various constraints. Following its initial implementation [3], research efforts have continued to advance the control of humanoid robots with the implementation of the WBC framework using experiment [4], [5], [6].

This work was supported by the National Research Foundation of Korea (NRF) grant funded by the Korea government (MSIT) (No. 2021R1A2C3005914). It was also supported by TUM AGENDA 2030, funded by the Federal Ministry of Education and Research (BMBF) and the Free State of Bavaria under the Excellence Strategy of the Federal Government and the Länder as well as by the Hightech Agenda Bavaria. (Corresponding Author: Jaeheung Park.)

¹J. Ahn, H. Lee and J. Park are with the Graduate School of Convergence Science and Technology, Seoul National University (SNU), Gwanak-ro 1, Gwanak-gu, Seoul, Republic of Korea. june992@snu.ac.kr, hkleetony@snu.ac.kr, park73@snu.ac.kr

²J. Jung is with Global Infrastructure and manufacturing, Samsung Electronics. jays.jung@samsung.com,

³Y. Lee is with the Korea Institute of Science and Technology (KIST), Seoul, 02792, Republic of Korea, yisoo.lee@kist.re.kr

⁴S. Haddadin is with Technical University of Munich, Germany; TUM School of Computation, Information and Technology (CIT); Chair of Robotics and Systems Intelligence (RSI); Munich Institute of Robotics and Machine Intelligence (MIRMI). haddadin@tum.de

⁵J. Park is also with ASRI, RICS, Seoul National University, Republic of Korea, and Advanced Institutes and Advanced Institutes of Convergence Technology(AICT), Republic of Korea.

Recent studies on whole-body control methods for walking robots have predominantly focused on optimization-based techniques, demonstrating significant improvements in control performance. One prominent method in this domain is Model Predictive Control (MPC), which predicts future states and optimizes trajectory accordingly. MPC has been implemented in various ways for humanoid robots, primarily in two major approaches. The first approach employs a whole-body model. Although substantial research has been conducted using whole-body models [7], [8], the complexity of these methods poses a major challenge in reducing computational burden [9], [10]. The second approach leverages simplified dynamic models such as centroidal dynamics [11], Linear inverted pendulum model [12], and Single Rigid Body Dynamics. Several research on MPC [13], [14] uses the simplified models and then extends the optimized trajectory of simplified model to the whole-body control. However, these simplified models have clear limitations, particularly in directly considering crucial contact constraints for walking robots.

The method of computing whole-body control inputs from the optimized trajectory of simplified model is known as instantaneous WBC (iWBC). Since the trajectory optimizations like MPC require significant computation time, it is crucial to reduce both the computation time and latency in iWBC to enhance performance. This latency is not merely a delay; it fundamentally undermines control stability, which is a critical concern highlighted in [15], [16].

Approaches to iWBC through optimization started with Quadratic Programming (QP), and the QP-based WBC formulation [17] takes into account robot dynamics and kinematics by considering multiple constraints and other practical conditions [18], [19], [20]. Subsequently, several studies [21], [22] utilized the Hierarchical Quadratic Programming (HQP), also known as Lexicographic QP (LQP), to maintain the explicit hierarchy of tasks and constraints. To reduce the computational burden of HQP, several methods have been proposed: A research [22] reduced computational cost by decomposing the optimization variables, especially the constraint by whole-body dynamics. Then [23] focused on developing solvers to reduce the computational load of HQP. Further, dedicated solvers [24], [25] for HQP were developed, achieving significant computational improvements.

Despite these advancements in solvers, many optimization-based control studies continue to rely on off-the-shelf optimization solvers. Solvers such as OSQP [26], qpOASES [27], acados [28], and quadprog are frequently used in research [13], [14], [29], [30], [31] due to the complexity

of developing custom solvers. These pre-built solvers facilitate optimization tasks by providing robust and efficient solutions, allowing researchers to focus on other aspects of control system design and implementation. From this perspective, the study [32] also formulated a lexicographic problem using the weighted method, demonstrating that significant performance improvements can be achieved with off-the-shelf solvers, even when compared with dedicated solvers.

Unlike conventional approaches to iWBC, a novel approach has been proposed in [33], [34], simplifying the constraint itself through operational space formulation. This approach resulted in a greater reduction in optimization variables and constraint dimension to previous methods [22], thus significantly enhancing computational performance even with the off-the-shelf optimization problem solvers. However, these methods not only consume additional computation time to construct the Operational Space Formulation (OSF) but also require a thorough understanding of the OSF. Moreover, inequality constraints in the joint space are considered indirectly through the operational space, which can potentially result in sub-optimal solutions.

This paper proposes a method that utilizes the projection into a specific space to split the dynamics model into two parts. The proposed method then solve the iWBC problem sequentially using the split models. The first part of the dynamics model proposed in this paper simplifies the joints that are not used to describe the constrained link, which typically associated with contact constraint. The dynamics of these unconstrained joints are summarized through centroidal dynamics, with a focus on environmental interaction, which is crucial for humanoid robots. For the second part, the dynamics of unconstrained link's joint space are considered. This two-part configuration allows the entire problem to be divided and addressed as two separate problems. The proposed method leverages the advantages of both whole-body dynamics and centroidal dynamics, offering a comprehensive approach to efficiently manage the computation problem.

The proposed method's approach is different from conventional approaches of iWBC by altering the fundamental dynamics model itself. The advantage of the proposed approach is that it allows the direct application of conventional methods, including solver-based methods, constraint handling, and optimization construction approaches, to our method.

The contributions of this study, which introduces a novel framework for improving efficiency, are as follows:

- Introduces a novel method for constructing reduced dimension rigid body dynamics in WBC, achieving high computational efficiency.
- Demonstrates how the reduced dynamics model can be integrated into various formulations of iWBC, providing a distinct approach that differentiates it from conventional methods to iWBC.

To elucidate these contributions, our paper is structured as follows: In Section II, a brief overview of the whole-body control knowledge is provided. Section III proposes new

novel method of constructing reduced dynamics. In Section IV the application of proposed method to conventional methods are introduced. The section V provides the result with the proposed method. Finally, Section VI concludes the paper with a discussion based on the validation findings.

II. CONSTRAINT FOR WHOLE-BODY CONTROL

Whole-body dynamics is a fundamental concept in robotics that expresses the dynamic behavior of a floating-base robot composed of multiple rigid bodies connected by joints. It describes how internal and external forces affect the robot's movements and can be expressed by the following equation:

$$\mathbf{M}(\mathbf{q})\ddot{\mathbf{q}} + \mathbf{b}(\mathbf{q}, \dot{\mathbf{q}}) + \mathbf{g}(\mathbf{q}) + \mathbf{J}_c(\mathbf{q})^T \mathbf{F}_c = \mathbf{S}^T \mathbf{\Gamma}, \quad (1)$$

where $\mathbf{q} \in \mathbb{R}^{n+6}$ is the generalized joint position vector of the system, and n is the degrees of freedom (DOF) of the robot actuated joints. $\mathbf{M}(\mathbf{q}) \in \mathbb{R}^{(n+6) \times (n+6)}$ is the inertia matrix, $\mathbf{b}(\mathbf{q}, \dot{\mathbf{q}}) \in \mathbb{R}^{n+6}$ is the Coriolis and centrifugal force vector, $\mathbf{g}(\mathbf{q}) \in \mathbb{R}^{n+6}$ is the gravity force vector, $\mathbf{S}^T \in \mathbb{R}^{(n+6) \times n}$ is a selection matrix that specifies actuated joints from system joints, $\mathbf{J}_c(\mathbf{q}) \in \mathbb{R}^{c \times (n+6)}$ is the constraint Jacobian, which usually used to describe the contact constraint of the robot. c is the constrained DOF, and $\mathbf{F}_c \in \mathbb{R}^c$ is a vector that concatenate all constraint forces.

The iWBC solves the optimization problem that considers whole-body dynamics to generate a feasible joint control solution when task space trajectories are given. Various inequality and equality constraints must be considered for the iWBC optimization problem. For a humanoid robot interacting with the external environment, the necessary constraints include the equality constraint with (1) to describe the robot's system dynamics. Additionally, the following inequality and equality constraints are required:

$$\text{(stationary contact)} \quad \mathbf{J}_c \dot{\mathbf{q}} = \dot{\mathbf{J}}_c \dot{\mathbf{q}} + \mathbf{J}_c \ddot{\mathbf{q}} = 0 \quad (2)$$

$$\text{(contact wrench cone)} \quad \mathbf{C} \mathbf{F}_c \leq 0 \quad (3)$$

$$\text{(task control)} \quad \mathbf{J}_{task} \ddot{\mathbf{q}} + \dot{\mathbf{J}}_{task} \dot{\mathbf{q}} = \ddot{\mathbf{x}}_{task}^{ref} \quad (4)$$

$$\text{(joint limits)} \quad \mathbf{\Gamma}_{min} < \mathbf{\Gamma} < \mathbf{\Gamma}_{max}, \dots \quad (5)$$

where \mathbf{J}_{task} is the task Jacobian and $\ddot{\mathbf{x}}_{task}^{ref}$ is a reference task acceleration that will correspond to a desired control method (e.g. LQR, MPC, or PD-controller), and \mathbf{C} is a matrix for a contact wrench cone that accounts for friction and CoP constraints.

The system dynamics constraint in (1) can be decomposed as proposed in [22], as follows,

$$\mathbf{M}_u \ddot{\mathbf{q}} + \mathbf{b}_u + \mathbf{g}_u + \mathbf{J}_{c,u}^T \mathbf{F}_c = 0 \quad (6)$$

$$\mathbf{M}_l \ddot{\mathbf{q}} + \mathbf{b}_l + \mathbf{g}_l + \mathbf{J}_{c,l}^T \mathbf{F}_c = \mathbf{\Gamma} \quad (7)$$

Equation (6) represents the top six equations of (1), and Equation (7) comprises the bottom n equations of (1). Equation (6) describes the Newton-Euler equations for the floating base and can be used as the dynamics constraint instead of (1). Through Equation (7), control torques, $\mathbf{\Gamma}$ can be calculated with $\ddot{\mathbf{q}}$ and \mathbf{F}_c . Therefore, by excluding torque

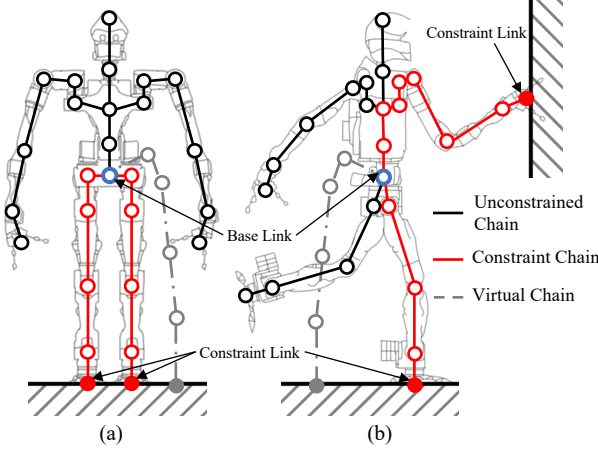


Fig. 1. Schematic representation of the robot model system, depicting the virtual chain, the constraint chain, and the unconstrained chain. In case of (a), the lower body forms the constraint chain while the upper body forms the unconstrained chain. In (b) the connected rigid bodies from the foot to the hand constitute the constraint chain, while the remaining parts—head, the other arm, and leg—form the unconstrained chain.

from the decision variable \mathbf{x} the optimization problem can be solved efficiently.

III. CONSTRUCTION OF UNCONSTRAINED IMPLICIT DYNAMICS

A. Categorization and Simplification of Kinematic Chains

In our method, we categorize the kinematic chain of floating-base robots into three types, as shown in Fig. 1. The first type is the *virtual chain*, which consists of virtual joints that describe the six DOF floating base body motion relative to the inertial frame. The second type is the n_{cc} -DOF *constraint chain*, which includes the kinematic chain between the base link and the links in constraint. These constraint links are typically described by \mathbf{J}_c , forming the constrained space (usually used as the contact space for walking robot). The third type is the n_{uc} -DOF *unconstrained chain*, which is the kinematic chain composed of the robot's links excluding the links included in the constraint chain.

In the proposed framework, the dynamical model of the unconstrained chain is simplified into six DOF utilizing the centroidal dynamics concept. Then, the n -DOF robot model can be reduced to $(n_{cc} + 12)$ -DOFs. The number 12 is from the summation of six DOF simplified unconstrained chain and six DOF virtual chain. The relationship between the original robot model and the reduced model can be seen in Fig. 2. Then the unconstrained chain is considered sequentially, resulting in the whole dynamics $(n + 6)$ -DOF being divided into two sequential problems: the reduced dynamics $(n_r + 6)$ -DOF and the unconstrained chain dynamics (n_{uc}) -DOF. The n_r denotes the DOF of actuated joints of reduced dynamics, which is $n_{cc} + 6$. Therefore, the proposed method decreases whole-body controller computational cost by reducing the DOF of the system dynamics and decision variable size.

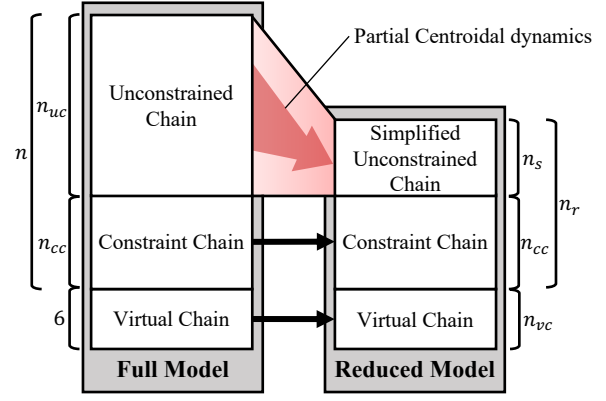


Fig. 2. Composition comparison between the ordinary robot model and the reduced-dimension robot model. The gray box on the left denotes the rigid-body dynamics model, and the gray box on the right denotes the reduced dimensional robot model. n is the DOF of the actuated joints of the original robot model, n_r is the DOF of the actuated joints of reduced dimensional model. n_{vc} , n_{cc} , n_{uc} represent the DOF of the virtual chain, constraint chain, and unconstrained chain, respectively. n_s is the DOF of the simplified unconstrained chain, which is six.

B. Interpreting Unconstrained Chain with Centroidal dynamics

The *centroidal dynamics* [11] describes the total linear momentum $\mathbf{l}_G \in \mathbb{R}^3$ and the total angular momentum $\mathbf{k}_G \in \mathbb{R}^3$ of the system. The centroidal momentum is composed as $\mathbf{h}_G = [\mathbf{k}_G^T \ \mathbf{l}_G^T]^T \in \mathbb{R}^6$.

Here, the centroidal dynamics is utilized to interpret the average movement of unconstrained chain. The centroidal momentum of the unconstrained chain, $\mathbf{h}_{G,uc}$ can be obtained with following,

$$\mathbf{h}_{G,uc} = \mathbf{M}_{G,uc}(\mathbf{q})\dot{\mathbf{q}}, \quad (8)$$

where $\mathbf{M}_{G,uc}(\mathbf{q}_{uc}) \in \mathbb{R}^{6 \times n_{uc}}$ is the *centroidal momentum matrix* [11] of the unconstrained chain. The centroidal momentum matrix describes the relationship between the joint coordinate and the centroidal momentum.

The average spatial velocity can be obtained with multiplying the inverse of the inertia matrix of the unconstrained chain with (8),

$$\mathbf{v}_{G,uc} = \mathbf{I}_{G,uc}^{-1} \mathbf{M}_{G,uc}(\mathbf{q}_{uc})\dot{\mathbf{q}}_{uc}. \quad (9)$$

Where $\mathbf{I}_{G,uc} \in \mathbb{R}^{6 \times 6}$ is the inertia matrix of the unconstrained chain.

With (9), the centroidal inertial Jacobian matrix of unconstrained chain that describes the relation between the average spatial velocity and joint space velocity can be obtained as follows:

$$\mathbf{J}_{G,uc} = \mathbf{I}_{G,uc}^{-1} \mathbf{M}_{G,uc}(\mathbf{q}_{uc}). \quad (10)$$

Consequently, it is possible to interpret the average spatial movement of unconstrained chain with (10).

C. Construction of Reduced Whole-Body Dynamics

By projecting the dynamics of the unconstrained chain into a six DOF centroidal space, the joint space can be

reconstructed as the reduced dimension vector \mathbf{q}_r .

$$\dot{\mathbf{q}}_r = \begin{bmatrix} \dot{\mathbf{q}}_{vc} \\ \dot{\mathbf{q}}_{cc} \\ {}^b\mathbf{v}_{G,uc} \end{bmatrix}, \quad (11)$$

where $\dot{\mathbf{q}}_{vc} \in \mathbb{R}^6$ is the generalized velocity of the virtual chain joints from an inertial frame, $\dot{\mathbf{q}}_{cc} \in \mathbb{R}^{n_{co}}$ is the generalized joint velocity of the constraint chain joints. The superscript preceding a variable denotes its reference frame. Here, ${}^b\mathbf{v}_{G,uc}$ indicates that $\mathbf{v}_{G,uc}$ is the spatial velocity of unconstrained chain relative to the reference frame of the robot base.

The term $\dot{\mathbf{q}}_r$ can be obtained from $\dot{\mathbf{q}}$ as follows by defining the matrix $\mathbf{J}_r \in \mathbb{R}^{n_r \times (n+6)}$.

$$\dot{\mathbf{q}}_r = \mathbf{J}_r \dot{\mathbf{q}}, \quad (12)$$

where

$$\mathbf{J}_r = \begin{bmatrix} \mathbf{S}_{vc} \\ \mathbf{S}_{cc} \\ {}^b\mathbf{J}_{G,uc}\mathbf{S}_{uc} \end{bmatrix}, \quad (13)$$

$\mathbf{S}_{vc} \in \mathbb{R}^{6 \times (n+6)}$, $\mathbf{S}_{cc} \in \mathbb{R}^{n_{cc} \times (n+6)}$, $\mathbf{S}_{uc} \in \mathbb{R}^{n_{uc} \times (n+6)}$ are selection matrices that select virtual chain, contact chain, and unconstrained chain joints from all joints, respectively. The centroidal inertial Jacobian matrix of the unconstrained chain ${}^b\mathbf{J}_{G,uc} \in \mathbb{R}^{6 \times n_{uc}}$ can be obtained from (10). The Jacobian matrix \mathbf{J}_r define the reduced-model space as task space.

With (12), the whole-body dynamics of the system (1) is projected into the reduced-model space,

$$\mathbf{M}_r \ddot{\mathbf{q}}_r + \mathbf{b}_r + \mathbf{g}_r + \mathbf{J}_{c,r}^T \mathbf{F}_c = \mathbf{S}_r^T \mathbf{\Gamma}_r, \quad (14)$$

where

$$\mathbf{M}_r = (\mathbf{J}_r \mathbf{M}^{-1} \mathbf{J}_r^T)^{-1}, \quad (14a)$$

$$\mathbf{b}_r = \mathbf{M}_r \{ \mathbf{J}_r \mathbf{M}^{-1} \mathbf{b} - \dot{\mathbf{J}}_r \dot{\mathbf{q}} \}, \quad (14b)$$

$$\mathbf{g}_r = \mathbf{M}_r \mathbf{J}_r \mathbf{M}^{-1} \mathbf{g}, \quad (14c)$$

$$\bar{\mathbf{J}}_r^T = \mathbf{M}_r \mathbf{J}_r \mathbf{M}^{-1}, \quad (14d)$$

$$\mathbf{J}_{c,r}^T = \bar{\mathbf{J}}_r^T \mathbf{J}_c^T. \quad (14e)$$

The matrix \mathbf{M}_r , \mathbf{b}_r , and \mathbf{g}_r are the projections of \mathbf{M} , \mathbf{b} , and \mathbf{g} into the reduced model space, respectively. $\bar{\mathbf{J}}_r^T$ denotes the dynamically consistent inverse of \mathbf{J}_r . $\mathbf{S}_r^T \in \mathbb{R}^{(n_r+6) \times n_r}$ is a selection matrix that specifies actuated joint for reduced model dynamics. $\mathbf{J}_{c,r}$ is the reduced-model space projection of contact Jacobian. Here, $\mathbf{J}_{c,r}^T$ can be more simply computed as

$$\mathbf{J}_{c,r}^T = \begin{bmatrix} \mathbf{S}_{vc} \\ \mathbf{S}_{cc} \\ \mathbf{0}_{6 \times (n+6)} \end{bmatrix} \mathbf{J}_c^T, \quad (15)$$

instead of (14e) since the contact Jacobian matrix inherently does not include components from the unconstrained chain.

Consequently, (14) can be considered a simplified representation of a system interacting with the external environment, and it can be utilized as equations of motion constraint for the reduced model in the iWBC method.

The effect of the unconstrained chain on the external environment can be described using (14), following the simplification process. Since the simplified model cannot capture the internal motion of the unconstrained chain, it's dynamics must also be described. By considering the unconstrained chain as an independent model, it's dynamics are given by:

$$\mathbf{M}_{uc} \ddot{\mathbf{q}}_{uc} + \mathbf{b}_{uc} + \mathbf{g}_{uc} = \mathbf{\Gamma}_{uc}, \quad (16)$$

where \mathbf{M}_{uc} is inertia matrix of the unconstrained chain, \mathbf{b}_{uc} is the Coriolis and centrifugal, and \mathbf{g}_{uc} is the gravity vector of unconstrained chain.

Through the process described in this subsection, the whole-body dynamics (1) can be divided into (14) and (16), thereby dividing the iWBC problem as well.

D. Motion Control Tasks via Reduced Dynamics Model

In the proposed method, task constraints are divided into two categories: those related to the reduced model joint space and those within the unconstrained chain.

1) Task Constraints in the Reduced Model Joint Space:

Tasks related to the robot's COM, and the tasks existing within the constraint chain fall into the first category. This also includes control of the upper body COM or the floating base. The relationship between the reference velocity in a specific task space and the joint velocities is given by:

$$\mathbf{J}_{task} \dot{\mathbf{q}} = \dot{\mathbf{x}}_{task}^{ref}, \quad (17)$$

where $\mathbf{J}_{task} \in \mathbb{R}^{m \times (n+6)}$ is the task space Jacobian matrix, $\dot{\mathbf{x}}_{task}^{ref} \in \mathbb{R}^m$ is the reference task space velocity vector, and m is the DOF of the task space.

The null-space projection matrix \mathbf{N}_r^T can be computed as follows:

$$\mathbf{N}_r^T = \mathbf{I} - \mathbf{J}_r^T \bar{\mathbf{J}}_r^T. \quad (18)$$

Using the identity $\mathbf{I} = \mathbf{N}_r^T + \mathbf{J}_r^T \bar{\mathbf{J}}_r^T$ from (18), the left-hand side of (17) can be represented as follows:

$$\mathbf{J}_{task} (\mathbf{N}_r + \bar{\mathbf{J}}_r \mathbf{J}_r) \dot{\mathbf{q}} = \dot{\mathbf{x}}_{task}^{ref}. \quad (19)$$

Expanding and rearranging (19) yields the following:

$$\mathbf{J}_{task} \mathbf{N}_r \dot{\mathbf{q}} + \mathbf{J}_{task} \bar{\mathbf{J}}_r \dot{\mathbf{q}}_r = \dot{\mathbf{x}}_{task}^{ref}. \quad (20)$$

When the task space exists within the constraints chain, or involves controlling robot's centroidal space or the centroidal space of the unconstrained chain, $\mathbf{J}_{task} \mathbf{N}_r \dot{\mathbf{q}} = 0$ holds true. This is because the joint velocity of the unconstrained chain, which do not affect the centroidal space of the unconstrained chain, does not influence these types of task space. Therefore, task spaces in these categories can describe $\dot{\mathbf{x}}_{task}^{ref}$ through $\dot{\mathbf{q}}_r$:

$$\mathbf{J}_{task} \bar{\mathbf{J}}_r \dot{\mathbf{q}}_r = \dot{\mathbf{x}}_{task}^{ref}. \quad (21)$$

These types of task constraints are considered in the first part of the iWBC problem, which is in the reduced model joint space.

2) *Task Constraints in the Unconstrained Chain:* The second category includes task spaces within the unconstrained chain. For these tasks, the constraints are established as:

$${}^b\mathbf{J}_{task,uc}\dot{\mathbf{q}}_{uc} = {}^b\dot{\mathbf{x}}_{task,uc}^{ref}, \quad (22)$$

where ${}^b\mathbf{J}_{task,uc} \in \mathbb{R}^{m \times n_{uc}}$ is the task Jacobian in the unconstrained chain relative to the reference frame of the robot base, and the ${}^b\dot{\mathbf{x}}_{task,uc}^{ref} \in \mathbb{R}^m$ is the reference task velocity from the reference frame of the robot base. The vector ${}^b\dot{\mathbf{x}}_{task,uc}^{ref}$ is computed based on the result of the first part of the problem, as it defines the movement of the robot base. Additionally, ${}^b\dot{\mathbf{x}}_{task,uc}^{ref}$ can also be defined by the task planner.

3) *Reference Acceleration Constraint:* The reference acceleration constraint in the task space, $\ddot{\mathbf{x}}_{task}^{ref}$, can be constructed by differentiating the reference velocity (20) above.

IV. PROBLEM FORMULATION

A. Lexicographic Quadratic Programming

The inequality and equality constraints for iWBC, can be expressed in affine form corresponding to the equality and inequality constraints at each level in an optimization problem consisting of p priorities,

$$\mathbf{A}_i\mathbf{x} + \mathbf{a}_i \leq 0, \mathbf{B}_i\mathbf{x} + \mathbf{b}_i = 0, i = 1, 2, \dots, p \quad (23)$$

All linear constraints from each priority can be combined and expressed as follows:

$$\underbrace{\begin{bmatrix} \mathbf{A}_1 \\ \vdots \\ \mathbf{A}_p \end{bmatrix}}_{\mathbf{A}}\mathbf{x} + \underbrace{\begin{bmatrix} \mathbf{a}_1 \\ \vdots \\ \mathbf{a}_p \end{bmatrix}}_{\mathbf{a}} \leq 0, \quad \underbrace{\begin{bmatrix} \mathbf{B}_1 \\ \vdots \\ \mathbf{B}_p \end{bmatrix}}_{\mathbf{B}}\mathbf{x} + \underbrace{\begin{bmatrix} \mathbf{b}_1 \\ \vdots \\ \mathbf{b}_p \end{bmatrix}}_{\mathbf{b}} = 0 \quad (24)$$

where $\mathbf{x} = [\ddot{\mathbf{q}}^T \mathbf{F}_c^T \mathbf{\Gamma}^T]^T$, $\mathbf{A} \in \mathbb{R}^{m_a \times (2n+6+6c)}$, $\mathbf{a} \in \mathbb{R}^{m_a}$, $\mathbf{B} \in \mathbb{R}^{m_b \times (2n+6+6c)}$, $\mathbf{b} \in \mathbb{R}^{m_b}$. m_a and m_b are the total number of inequality and equality constraints of all priorities, respectively. c is the number of contact links.

With the constraints formulation above, LQP [24] is formulated as follows:

$$\min_{\mathbf{x}, \mathbf{v}, \mathbf{w}} \|\mathbf{v}\|^2 + \|\mathbf{w}\|^2 \quad (25)$$

$$\text{s.t. } \mathbf{V}(\mathbf{Ax} + \mathbf{a}) \leq \mathbf{v} \quad (25a)$$

$$\mathbf{W}(\mathbf{Bx} + \mathbf{b}) = \mathbf{w} \quad (25b)$$

where $\mathbf{V} \in \mathbb{R}^{m_a \times m_a}$, $\mathbf{W} \in \mathbb{R}^{m_b \times m_b}$ are weight matrices of inequality and equality constraints, respectively, and $\mathbf{v} \in \mathbb{R}^{m_a}$, $\mathbf{w} \in \mathbb{R}^{m_b}$ are slack variables for inequality and equality constraints, respectively.

This formulation of the LQP problem can be solved by hierarchical method [35] or weighted method [32], [36]. The sequential method utilizes the null space basis matrix of the higher priority's equality constraint matrix to maintain the higher priority's constraint and uses the previously computed slack variables for the inequality constraints. The weighted method performs optimization by appropriately utilizing weighting matrices to ensure that constraints at higher priority levels receive more focus.

B. LQP Formulation with Reduced Dynamics

The optimization problem utilizing the reduced dynamics is divided into two parts: LQP 1 and LQP 2. LQP 1 uses the reduced dimension dynamics as constraints to account for interactions with the external environment. LQP 2 deals with the control of the unconstrained chain, based on the constraint of the simplified unconstrained chain determined by the solution of the LQP 1.

In both parts, we construct a cost function to calculate the movement that minimizes the robot's *acceleration energy* [37], \mathbf{E}_a . The acceleration energy of the robot is defined as follows:

$$\mathbf{E}_a = \frac{1}{2} \ddot{\mathbf{q}}^T \mathbf{M} \ddot{\mathbf{q}}. \quad (26)$$

The first part of the optimization problem, LQP 1, utilizing the reduced dimension dynamics, is formulated similarly to (25) as follows,

$$\min_{\ddot{\mathbf{q}}_r, \mathbf{F}_c, \mathbf{v}, \mathbf{w}} \ddot{\mathbf{q}}_r^T \mathbf{M}_r \ddot{\mathbf{q}}_r + \|\mathbf{v}\|^2 + \|\mathbf{w}\|^2 \quad (27)$$

$$\text{s.t. } \mathbf{V}(\mathbf{Ax} + \mathbf{a}) \leq \mathbf{v} \quad (27a)$$

$$\mathbf{W}(\mathbf{Bx} + \mathbf{b}) = \mathbf{w} \quad (27b)$$

Similar to how (6) is considered as a constraint in the original joint space, the reduced model dynamics (14) also consider only the top six rows of equations as constraints, resulting in the exclusion of torque from the decision variables.

Equations (27a) and (27b) represent the constraints mentioned in Section II, formulated through reduced dynamics. For the task space, the constraints are constructed using the reduced dynamics, as discussed in subsection III-D, which can only be composed through such task constraints.

The given solution $\ddot{\mathbf{q}}_r^*$ of LQP 1 (27) are utilized in the second problem, LQP 2. From the $\ddot{\mathbf{q}}_r^* = [(\ddot{\mathbf{q}}_{uc}^*)^T \ddot{\mathbf{q}}_{cc}^T ({}^b\ddot{\mathbf{x}}_{G,uc}^*)^T]^T$, $\ddot{\mathbf{q}}_{vc}^* \in \mathbb{R}^6$, $\ddot{\mathbf{q}}_{cc}^* \in \mathbb{R}^{n_{cc}}$ denotes the floating base spatial acceleration, joint acceleration of contact chain, respectively, and ${}^b\ddot{\mathbf{x}}_{G,uc}^* \in \mathbb{R}^6$ denotes the spatial acceleration of the unconstrained chain's centroidal space in the base frame.

The second part of optimization problem to handle the unconstrained chain, LQP 2, is,

$$\min_{\ddot{\mathbf{q}}_{uc}, \mathbf{v}_{uc}, \mathbf{w}_{uc}} \ddot{\mathbf{q}}_{uc}^T \mathbf{M}_{uc} \ddot{\mathbf{q}}_{uc} + \|\mathbf{v}_{uc}\|^2 + \|\mathbf{w}_{uc}\|^2 \quad (28)$$

$$\text{s.t. } \dots \text{ (other equality and inequality constraints)} \quad (28a)$$

where \mathbf{v}_{uc} and \mathbf{w}_{uc} are the constraint slack variables for unconstrained chain. The constraints of LQP 2 are also formulated with similar to (27a), and (27b).

The important constraint in (28a) is the equality constraint with the unconstrained chain's centroidal space, utilizing the solutions in LQP 1, ${}^b\ddot{\mathbf{x}}_{G,uc}^*$,

$${}^b\mathbf{J}_{G,uc}\ddot{\mathbf{q}}_{uc} + {}^b\dot{\mathbf{J}}_{G,uc}\dot{\mathbf{q}}_{uc} = {}^b\ddot{\mathbf{x}}_{G,uc}^*. \quad (29)$$

With this equality constraint, the solution of LQP 2 does not affect the LQP 1, (27).

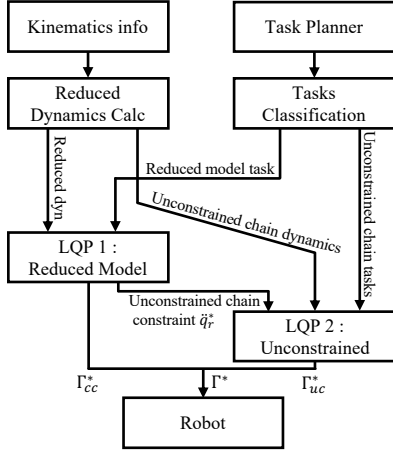


Fig. 3. The algorithm flow chart utilizing the proposed reduced dynamics.

For the task space constraint in the unconstrained chain, the desired acceleration of task space ${}^b\ddot{\mathbf{x}}_{i,uc}^{ref}$ is calculated from the reference task acceleration $\ddot{\mathbf{x}}_v^{ref}$ and the acceleration of the floating base, $\ddot{\mathbf{q}}_{vc}$ obtained from the LQP 1. This allows for the computation of the desired acceleration ${}^b\ddot{\mathbf{x}}_{i,uc}^{ref}$ of the task relative to the robot base. The overall flow of the calculation process can be seen in Fig. 3.

Depending on the priority of the unconstrained chain's tasks, which may take precedence over the centroidal space task, (29) might need to be violated. This violation can be calculated in LQP 2 through the corresponding slack variables of constraint (29), $\mathbf{W}_{G,uc}^{-1} \mathbf{w}_{G,uc}^*$, and these violations can then be incorporated as an additional priority in LQP 1. Although the inclusion of this additional priority increases the computational load, the increase is not significant.

The constraint chain control torque $\Gamma_{cc}^* \in \mathbb{R}^{n_{cc}}$ from the computation result of LQP 1 and the unconstrained chain control torque $\Gamma_{uc}^* \in \mathbb{R}^{n_{uc}}$ from the LQP 2 are used to construct the control torque input of the robot $\Gamma^* = [\Gamma_{cc}^{*T} \Gamma_{uc}^{*T}]^T$.

V. EVALUATION

A. System Setup

To validate the efficiency and performance of the method proposed in this paper, we employed the two-level computation framework to configure an HQP controller and compared its performance with that of a conventional HQP controller. The proposed framework was validated through the simulation. The robot used in the simulation, TOCABI, is human-sized (1.8m in height, 100kg in weight), 33-DOF torque-controlled humanoid robot. It is equipped with eight DOFs in each arm, six in each leg, three in the waist, and two in the head. The experiment was conducted on i7-10700 CPU, with the simulator MuJoCo. For the QP solver, one of the off-the-shelf solvers, OSQP, was used. The robot's operating system is Ubuntu 20.04, with a real-time patch applied using Xenomai 3.2.1. Further detailed information about the robot and system configuration can be found in [38].

TABLE I
TASK CONFIGURATION WITH CONVENTIONAL METHOD

Priority	Task	Size of constraint
1	Dynamics constraint (6)	6 eq
	Torque limit	$2 \times n$ ineq
2	Contact constraint	$6 \times c$ eq
	CoP & friction cone	$10 \times c$ ineq
3	Joint acceleration limit	$2 \times n$ ineq
	COM position	3 eq
4	Pelvis Orientation	3 eq
	End effector position & orientation	$6 \times k$ eq
decision variable size : $(n + 6) + 6 \times c$		

TABLE II
TASK CONFIGURATION WITH PROPOSED METHOD

Priority	Task	Size of constraint
LQP 1	Dynamics constraint (14)	6 eq
	Torque limit	$2 \times n_r$ ineq
	Contact constraint	$6 \times c$ eq
	CoP & friction cone	$10 \times c$ ineq
	Joint acceleration limit	$2 \times n_r$ ineq
3	COM position	3 eq
	Pelvis Orientation	3 eq
decision variable size : $(n_r + 6) + 6 \times c$		
LQP 2	unconstrained chain centroidal acceleration	6 eq
	Torque limit	$2 \times n_{uc}$ ineq
	End effector position & orientation	$6 \times k$ eq
	Joint acceleration limit	$2 \times n_{uc}$ ineq
decision variable size : n_{uc}		

B. Result with Proposed Method

The task for comparative experiments is configured as seen in Table I. These tasks were constructed similarly to the tasks in [22], for bipedal robot walking. Table I shows the various task hierarchies of LQP formulation configured using the original whole-body model. Since the walking consists of single contact and double contact scenarios, Table II shows how the tasks from Table I are divided into two parts utilizing the proposed method. The result measured the computation time in single support ($c = 1, k = 2$) and double support ($c = 2, k = 1$) scenarios occurring during walking. The tasks configured in this manner were structured in an LQP formulation and computed through the sequential method.

The results of comparing the computation times for solving the LQP problem using the sequential method can be observed in Table III.

Table III compares the average computation times of the conventional method and the proposed method during double contact and single contact scenarios. In both scenarios, the proposed method demonstrated an improvement in computational performance, with a 299% increase in the single support scenario and a 222% increase in the double support scenario, indicating enhanced performance compared to the original computation times.

The trajectory tracking errors resulting from task control using the proposed method and the conventional method were measured and compared. The COM and end-effector of the arm are controlled at the same time. The control errors can be observed in Figure 4. Similar magnitudes of control error were observed in both methods. Task space control

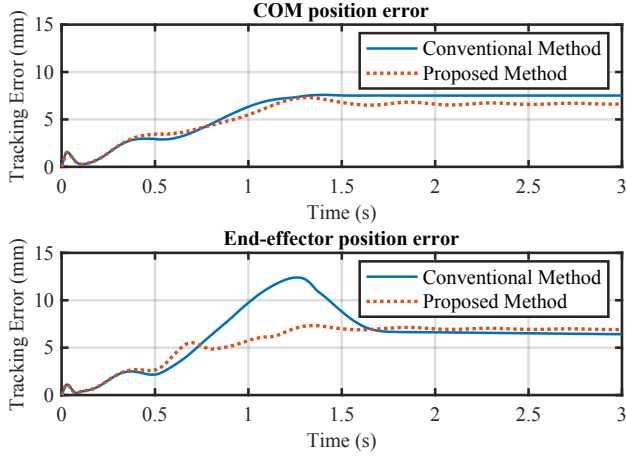


Fig. 4. Tracking errors of COM and end-effector positions using conventional and proposed methods. The tracking error was measured by controlling the robot during double support.

performance varies with the tuning of the weighting matrix, making it challenging to compare the two methods under perfectly identical conditions. Nevertheless, it can be seen that both methods achieve a comparable level of control.

TABLE III
COMPARISON OF COMPUTATION TIMES WITH SUPPORT TYPES

Support Type	Method	Total AVG	Total Max	Dyn Calc	LQP 1	LQP 2
Double	Conventional	2176 μ s	2473 μ s	-	-	-
	Proposed	981 μ s	1203 μ s	34 μ s	579 μ s	273 μ s
Single	Conventional	1834 μ s	2119 μ s	-	-	-
	Proposed	613 μ s	811 μ s	36 μ s	243 μ s	270 μ s

C. Computational Performance Analysis by DOF

The proposed method was also analyzed to determine its impact on the computational performance of LQP based on the robot's DOF. With both feet in contact, the benchmark examined how changing the DOF in the upper body affected computational performance.

Task configuration for the comparison is also set up similar to Table I and Table II. The difference lies in the task within the unconstrained chain. The end-effector of the arm is defined as the task space.

Benchmark tests were conducted by varying the robot model's DOF from 20 to 45, and the results are displayed in Figure 5. When tested on a 20-DOF robot model, the proposed method took 571 μ s, while the conventional method required an average computation time of 754 μ s, showing a 132% improvement in computational performance. This computational performance improvement increases with the robot model's DOF. When tested on a 45-DOF robot model, the proposed method took only 1319 μ s, while the conventional method required 4081 μ s, resulting in a 310% improvement in computational efficiency.

VI. CONCLUSIONS

In this study, a novel method for constructing reduced-dimension rigid body dynamics is proposed. This method

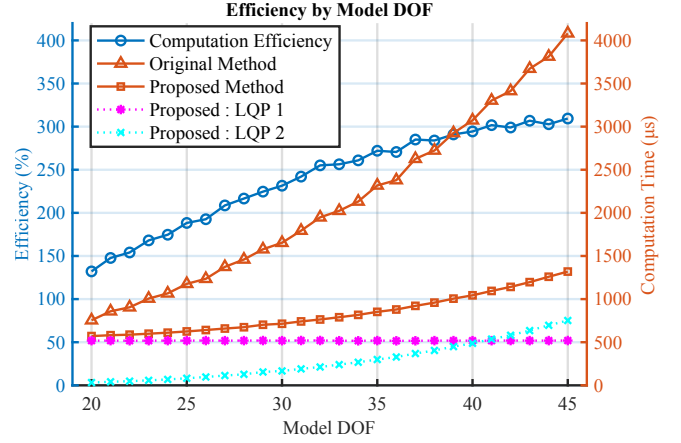


Fig. 5. Average computation time comparison by DOF of the robot, and the relative computation time percentage. The computation efficiency is measured by calculating the percentage ratio of the computation time of the original method to the computation time of the proposed method, using : (Original Method/Proposed Method) \times 100%. The computation time of proposed method is composed of computation time of LQP 1 and LQP 2.

employs a reduced-dimension dynamics based on constraints of the kinematic chain, partially projecting the unconstrained kinematic chain into its centroidal space, aiming to improve computational efficiency. The proposed method offers a unique approach by dividing the model into two parts with lower DOF, thereby enhancing computational efficiency by handling lower-DOF models in each sequence of the problem.

This strategy distinguishes the proposed method from conventional approaches to iWBC by focusing on dynamics simplification, which allows for the application of conventional methods of iWBC. The proposed method is integrated with LQP-based problems using the sequential method with off-the-shelf solvers. It is also available to use other solving method of LQP, or integrate the other dedicated solvers for the LQP.

When the proposed method was applied to the LQP formulation, which is commonly used in other studies, and computed using the sequential method, a 222 % improvement in computational efficiency was observed for the 33-DOF model at double support, and a 310% improvement was observed for the 45-DOF model. This demonstrates a significant performance improvement with increasing DOF. The control performance was also found to be similar between the two methods, demonstrating that computational time can be reduced without compromising control performance.

For the future works, we would also like to develop this method for higher-level planners to tackle more complex computational challenges.

REFERENCES

- [1] J. Park and O. Khatib, "Contact consistent control framework for humanoid robots," in *Proc. 2006 IEEE Int. Conf. Robot. and Automat. (ICRA)*, 2006, pp. 1963–1969.
- [2] L. Sentis and O. Khatib, "A whole-body control framework for humanoids operating in human environments," in *Proceedings 2006 IEEE International Conference on Robotics and Automation, 2006. ICRA 2006*. IEEE, 2006, pp. 2641–2648.

- [3] B. Stephens, *Push recovery control for force-controlled humanoid robots*. Carnegie Mellon University, 2011.
- [4] Y. Lee, S. Hwang, and J. Park, "Balancing of humanoid robot using contact force/moment control by task-oriented whole body control framework," *Autonomous Robots*, vol. 40, pp. 457–472, 2016.
- [5] D. Kim, Y. Zhao, G. Thomas, B. R. Fernandez, and L. Sentis, "Stabilizing series-elastic point-foot bipeds using whole-body operational space control," *IEEE Transactions on Robotics*, vol. 32, no. 6, pp. 1362–1379, 2016.
- [6] Y. Lee, H. Lee, J. Lee, and J. Park, "Toward reactive walking: Control of biped robots exploiting an event-based fsm," *IEEE Transactions on Robotics*, vol. 38, no. 2, pp. 683–698, 2021.
- [7] J. Koenemann, A. Del Prete, Y. Tassa, E. Todorov, O. Stasse, M. Bennis, and N. Mansard, "Whole-body model-predictive control applied to the hrp-2 humanoid," in *2015 IEEE/RSJ International Conference on Intelligent Robots and Systems (IROS)*. IEEE, 2015, pp. 3346–3351.
- [8] M. Neunert, M. Stuble, M. Gifftthaler, C. D. Bellicoso, J. Carius, C. Gehring, M. Hutter, and J. Buchli, "Whole-body nonlinear model predictive control through contacts for quadrupeds," *IEEE Robotics and Automation Letters*, vol. 3, no. 3, pp. 1458–1465, 2018.
- [9] S. Katayama, M. Murooka, and Y. Tazaki, "Model predictive control of legged and humanoid robots: models and algorithms," *Advanced Robotics*, vol. 37, no. 5, pp. 298–315, 2023.
- [10] P. M. Wensing, M. Posa, Y. Hu, A. Escande, N. Mansard, and A. Del Prete, "Optimization-based control for dynamic legged robots," *IEEE Transactions on Robotics*, 2023.
- [11] D. E. Orin, A. Goswami, and S.-H. Lee, "Centroidal dynamics of a humanoid robot," *Autonomous robots*, vol. 35, pp. 161–176, 2013.
- [12] S. Kajita, F. Kanehiro, K. Kaneko, K. Yokoi, and H. Hirukawa, "The 3d linear inverted pendulum mode: A simple modeling for a biped walking pattern generation," in *IEEE/RSJ International Conference on Intelligent Robots and Systems. Expanding the Societal Role of Robotics in the Next Millennium*, vol. 1, 2001, pp. 239–246.
- [13] N. Rathod, A. Bratta, M. Focchi, M. Zanon, O. Villard, C. Semini, and A. Bemporad, "Model predictive control with environment adaptation for legged locomotion," *IEEE Access*, vol. 9, pp. 145 710–145 727, 2021.
- [14] S. H. Jeon, S. Kim, and D. Kim, "Online optimal landing control of the mit mini cheetah," in *2022 International Conference on Robotics and Automation (ICRA)*. IEEE, 2022, pp. 178–184.
- [15] G. Stepan and T. Insperger, "Stability of time-periodic and delayed systems—a route to act-and-wait control," *Annual reviews in control*, vol. 30, no. 2, pp. 159–168, 2006.
- [16] J. Jung, S. Hwang, Y. Lee, J. Sim, and J. Park, "Analysis of position tracking in torque control of humanoid robots considering joint elasticity and time delay," in *2017 IEEE-RAS 17th International Conference on Humanoid Robotics (Humanoids)*. IEEE, 2017, pp. 515–521.
- [17] C. Collette, A. Micaelli, C. Andriot, and P. Lemerle, "Robust balance optimization control of humanoid robots with multiple non coplanar grasps and frictional contacts," in *2008 IEEE International Conference on Robotics and Automation*. IEEE, 2008, pp. 3187–3193.
- [18] S. Feng, E. Whitman, X. Xinjilefu, and C. G. Atkeson, "Optimization-based full body control for the darpa robotics challenge," *Journal of field robotics*, vol. 32, no. 2, pp. 293–312, 2015.
- [19] S. Kuindersma, F. Permenter, and R. Tedrake, "An efficiently solvable quadratic program for stabilizing dynamic locomotion," in *2014 IEEE International Conference on Robotics and Automation (ICRA)*. IEEE, 2014, pp. 2589–2594.
- [20] G. Mesesan, J. Engelsberger, G. Garofalo, C. Ott, and A. Albu-Schaffer, "Dynamic walking on compliant and uneven terrain using dcm and passivity-based whole-body control," in *2019 IEEE-RAS 19th International Conference on Humanoid Robots (Humanoids)*. IEEE, 2019, pp. 25–32.
- [21] M. De Lasa and A. Hertzmann, "Prioritized optimization for task-space control," in *2009 IEEE/RSJ International Conference on Intelligent Robots and Systems*. IEEE, 2009, pp. 5755–5762.
- [22] A. Herzog, N. Rotella, S. Mason, F. Grimmering, S. Schaal, and L. Righetti, "Momentum control with hierarchical inverse dynamics on a torque-controlled humanoid," *Autonomous Robots*, vol. 40, pp. 473–491, 2016.
- [23] M. De Lasa, I. Mordatch, and A. Hertzmann, "Feature-based locomotion controllers," *ACM transactions on graphics (TOG)*, vol. 29, no. 4, pp. 1–10, 2010.
- [24] A. Escande, N. Mansard, and P.-B. Wieber, "Hierarchical quadratic programming: Fast online humanoid-robot motion generation," *The International Journal of Robotics Research*, vol. 33, no. 7, pp. 1006–1028, 2014.
- [25] D. Dimitrov, A. Sherikov, and P.-B. Wieber, "Efficient resolution of potentially conflicting linear constraints in robotics," 2015. [Online]. Available: <https://hal.inria.fr/hal-01183003>
- [26] B. Stellato, G. Banjac, P. Goulart, A. Bemporad, and S. Boyd, "OSQP: an operator splitting solver for quadratic programs," *Mathematical Programming Computation*, vol. 12, no. 4, pp. 637–672, 2020. [Online]. Available: <https://doi.org/10.1007/s12532-020-00179-2>
- [27] H. Ferreau, C. Kirches, A. Potschka, H. Bock, and M. Diehl, "qpOASES: A parametric active-set algorithm for quadratic programming," *Mathematical Programming Computation*, vol. 6, no. 4, pp. 327–363, 2014.
- [28] R. Verschuere, G. Frison, D. Kouzoupis, J. Frey, N. van Duijkeren, A. Zanelli, B. Novoselnik, T. Albin, R. Quirynen, and M. Diehl, "acados – a modular open-source framework for fast embedded optimal control," *Mathematical Programming Computation*, 2021.
- [29] G. Raiola, E. Mingo Hoffman, M. Focchi, N. Tsagarakis, and C. Semini, "A simple yet effective whole-body locomotion framework for quadruped robots," *Frontiers in Robotics and AI*, vol. 7, p. 528473, 2020.
- [30] V. Klemm, A. Morra, L. Gulich, D. Mannhart, D. Rohr, M. Kamel, Y. de Viragh, and R. Siegwart, "Lqr-assisted whole-body control of a wheeled bipedal robot with kinematic loops," *IEEE Robotics and Automation Letters*, vol. 5, no. 2, pp. 3745–3752, 2020.
- [31] N. Ramuzat, G. Buondonno, S. Boria, and O. Stasse, "Comparison of position and torque whole-body control schemes on the humanoid robot talos," in *2021 20th International Conference on Advanced Robotics (ICAR)*. IEEE, 2021, pp. 785–792.
- [32] A. S. Sathya, G. Pipeleers, W. Decre, and J. Swevers, "A weighted method for fast resolution of strictly hierarchical robot task specifications using exact penalty functions," *IEEE Robotics and Automation Letters*, vol. 6, no. 2, pp. 3057–3064, 2021.
- [33] Y. Lee, S. Kim, J. Park, N. Tsagarakis, and J. Lee, "A whole-body control framework based on the operational space formulation under inequality constraints via task-oriented optimization," *IEEE Access*, vol. 9, pp. 39 813–39 826, 2021.
- [34] Y. Lee, J. Ahn, J. Lee, and J. Park, "Computationally efficient hqp-based whole-body control exploiting the operational-space formulation," in *2021 IEEE/RSJ International Conference on Intelligent Robots and Systems (IROS)*, 2021, pp. 5197–5202.
- [35] A. Herzog, S. Schaal, and L. Righetti, "Structured contact force optimization for kino-dynamic motion generation," in *2016 IEEE/RSJ International Conference on Intelligent Robots and Systems (IROS)*. IEEE, 2016, pp. 2703–2710.
- [36] H. D. Sherali, "Equivalent weights for lexicographic multi-objective programs: Characterizations and computations," *European Journal of Operational Research*, vol. 11, no. 4, pp. 367–379, 1982.
- [37] H. Bruyninckx and O. Khatib, "Gauss' principle and the dynamics of redundant and constrained manipulators," in *IEEE International Conference on Robotics and Automation. Millennium Conference.*, vol. 3, 2000, pp. 2563–2568.
- [38] J. Ahn, S. Park, J. Sim, and J. Park, "Dual-channel ethercat control system for 33-dof humanoid robot tocabi," *IEEE Access*, vol. 11, pp. 44 278–44 286, 2023.